Applied Catalysis B: Environmental 160–161 (2014) 390–399

Contents lists available at ScienceDirect

Applied Catalysis B: Environmental

journal homepage: www.elsevier.com/locate/apcatb

Comparative surface analysis and TAP measurements to probe the NO adsorptive properties of natural gas vehicle Pd–Rh/Al_2O_3 catalyst

Y. Renème[a], F. Dhainaut[a,b], Y. Schuurman[c], C. Mirodatos[c], P. Granger[a,*]

[a] Unité de Catalyse et de Chimie du Solide (UCCS), UMR CNRS 8181, Université Lille 1 Sciences et Technologies, Villeneuve d'Ascq, France
[b] Ecole Nationale Supérieure de Chimie de Lille, bâtiment C3, 59650 Villeneuve d'Ascq, France
[c] Ircelyon, Institut de Recherches sur la Catalyse et l'Environnement de Lyon, UMR 5256, 2, Avenue Albert Einstein, 69626 Villeurbanne Cedex, France

ARTICLE INFO

Article history:
Received 23 March 2014
Received in revised form 21 May 2014
Accepted 24 May 2014
Available online 2 June 2014

Keywords:
Thermal ageing
TAP reactor
Bimetallic Pd–Rh catalyst
$DeNO_x$ reaction
NGV catalyst

ABSTRACT

Thermal ageing has a significant detrimental effect on the behavior of bimetallic Pd–Rh natural gas fuelled vehicle (NGV) catalysts toward NO adsorption and its dissociation recognized as structure-sensitive. The ageing procedure at the lab-scale consisted of a thermal treatment under wet atmosphere (10 vol.% H_2O in air) at 980 °C that would induce comparable surface reconstructions taking place under real exhaust conditions of Pd–Rh/Al_2O_3 catalysts. XPS and FTIR of CO adsorption highlight the occurrence of simultaneous particle sintering and preferential surface Rh enrichment. Temporal analysis of product (TAP) experiments have been implemented for in situ characterization that allows the elucidation of surface reactions and diffusion processes taking place at the surface of Pd–Rh/Al_2O_3 when single NO pulse is introduced. It was found that the relative rates of those processes are strongly affected by the dispersion and the Rh composition on freshly-prepared and aged catalysts. Interestingly, Rh recognized as the most suitable noble metal to convert NO to N_2 would also slow down the agglomeration on Pd further protecting the metal/support interface.

1. Introduction

The reduction of NO emissions in post-combustion catalysis has recently attracted a growing interest at low temperature typically during the cold start of stoichiometric Natural gas fuelled vehicles (NGV) [1–6]. Generally, below an optimum temperature, NO is incompletely reduced, producing significant amount of nitrous oxide (N_2O) [7,8]. Such a trend was also reported on aged three ways catalysts (TWC). Up to now, N_2O emissions are not regulated but its strong greenhouse gas effect (300 times higher than that of CO_2) stimulates car manufacturers to anticipate more restrictive standard regulations and develop more efficient catalysts during the cold start engine with higher durability in three-way conditions. Typically, NGV catalysts are mainly composed of palladium and rhodium, which accomplish the most prominent reactions at the surface related to the simultaneous removal of methane and NO_x under cycling lean/rich conditions. Previous paper on the same catalyst dealt with the methane conversion from TAP experiments showing different behavior toward methane adsorption according to the surface coverage of oxygen atoms [9]. Indeed, Bounechada et al. [5] found different product distributions under lean or rich conditions with complete oxidation of H_2, CO, CH_4 and NO in large excess of oxygen whereas NO reduction, steam reforming and water gas shift reactions take place in rich conditions. The possible contribution of different oxygen species has been previously underlined [10,11] when Pd interacts with oxygen [12] leading to the formation of chemisorbed oxygen on metallic Pd, surface palladium oxide and subsurface palladium oxide. Time-resolved in situ XANES spectroscopy and DFT calculations also led to the conclusion that an intermediate atomic O/Pd ratio is needed to get an optimal activity for methane conversion, an oxygen-rich surface hindering the dissociative adsorption of methane [11]. However, the most prominent observations were related to the involvement of the metal/support interface since under reducing conditions, OH groups coming from the support may activate methane chemisorbed on Pd. All these surface modifications can also considerably alter the efficiency of NGV three-way catalysts toward NO conversion to nitrogen suppressing the metal/support interface and enhancing the production of N_2O as previously demonstrated for gasoline TWC [12]. As a general trend, more complex kinetic features characterize bimetallic catalysts as reported elsewhere especially when Rh is associated to Pt or Pd with different intrinsic affinity toward NO adsorption and dissociation [3]. Typically, under oscillating conditions,

* Corresponding author. Tel.: +33 3 20 43 49 38; fax: +33 3 20 43 65 61.
E-mail address: pascal.granger@univ-lille1.fr (P. Granger).

http://dx.doi.org/10.1016/j.apcatb.2014.05.046
0926-3373/

with alternative reductive/oxidative atmospheres, changes in the surface composition of TWCs currently occur especially at high temperature. Hence, irreversible phenomena can take place, which considerably modify the adsorptive properties of noble metals because of preferential surface enrichment [12]. Structural changes associated to the morphology of metallic particles can also induce significant modifications since NO dissociation is structure sensitive [13]. Interestingly, Peden et al. [13] found that the rate of NO conversion on Rh(1 1 0) is between 1.3 and 6.3 times faster than over Rh(1 1 1). This behavior was attributed to a much more facile NO dissociation on a less dense Rh(1 1 0) surface. Such a behavior is also accompanied with large differences in N_2 selectivity because higher N atom coverage on the (1 1 0) surface favors the recombination of N atoms.

Based on these previous findings, particular attention has been paid in this paper to the relative impact of thermal ageing on the adsorption of NO and subsequent surface reactions taking place on Pd–Rh/Al_2O_3 in a fast pulsed TAP reactor under ultra-high-vacuum (UHV), allowing surface science analysis on an industrial catalyst [14,15]. Single NO pulse TAP experiments were carried out to investigate the possible changes in reactivity of adsorbates related to surface Rh enrichment and to the extent of metal/support interface. Changes in selectivity behavior will be discussed based on previous steady-state kinetic measurements performed on the same catalysts at atmospheric pressure. The gained information was analyzed together with surface characterization from XPS analysis and CO infrared spectroscopic measurements, in order to provide a straightforward visualization of the impact of thermal ageing on the surface properties of aged Pd–Rh/Al_2O_3.

2. Experimental

2.1. Catalyst preparation and surface characterization

Bimetallic supported Pd and Rh-based catalysts supplied by Umicore were synthesized via a classical wet impregnation of γ-Al_2O_3 support (250 $m^2\ g^{-1}$) with aqueous rhodium and palladium nitrate solutions to obtain ultimately 2.5 and 0.18 wt.% palladium and rhodium, respectively [3,16]. Impregnated samples were successively calcined in air at 500 °C for 4 h. Thermal ageing was performed at 980 °C on calcined samples under controlled atmosphere in the presence of 10 vol.% H_2O diluted in air.

Metal dispersion was calculated from H_2 titration performed at 100 °C to avoid the formation of palladium hydride [17] using a pulse technique on pre-reduced catalysts in pure H_2 at 500 °C and assuming an atomic H/M ratio ~ 1 (M = Pd and Rh) (see Table 1).

XPS experiments were carried out on calcined and aged catalysts in a Vacuum Generators Escalab 220XL spectrometer under ultra-high-vacuum (~10^{-10} Torr) equipped with a monochromatic aluminum source for excitation. Samples were preliminary in situ reduced at 500 °C in pure hydrogen prior to XPS measurements. Binding energy (B.E.) values were referenced to the binding energy of the Al 2p core level (74.6 eV in Al_2O_3). Simulation of the experimental photopeaks was carried out using a mixed Gaussian/Lorentzian peak fit procedure and a non-linear Shirley background subtraction [18,19].

CO chemisorption was investigated by infrared spectroscopy on pre-reduced samples overnight in pure H_2 at 450 °C and further degassed in helium at the same temperature. IR spectra were recorded at room temperature under 1 vol.% CO diluted in He. A Nicolet 460 FTIR spectrometer fitted with a MCT detector and equipped with a DRIFT cell supplied by Harrick was used.

2.2. Temporal analysis of product (TAP) experiments

Transient measurements were carried out in a TAP-2 set-up reactor described elsewhere [20] with experiments performed in the Knudsen regime. Under these conditions, only surface reaction steps take place excluding gas phase reactions. The reactor with a diameter size of 4 mm and a length of 2.54 cm was composed of three different zones: 220 mg (or 1 cm long) of quartz, 20 mg (or 0.48 cm) of catalysts and 235 mg of quartz (1.06 cm). Prior to multi-pulse experiments, the catalyst was exposed to a 100 successive H_2 pulses exposure at 400 °C to get a clean reduced surface before each experiment, or by using the slide valve from the TAP-2 set-up, which was used to isolate the microreactor from the UHV chamber and then the catalyst was heated at atmospheric pressure under reductive conditions. Each pulse contained 6×10^{15} molecules of active gas (NO or O_2). Single pulse experiments (SP) were performed on stabilized surfaces corresponding to steady-state NO conversion after 100 successive single pulses. Calibration of the mass spectrometer was done for the m/z responses relative to Ar, N_2, NO, NO_2, O_2, and N_2O. The duration between two successive NO/Ar pulses was adapted varying between 1.5 and 2 s for returning to the baseline value.

3. Results and discussion

3.1. Surface analysis of fresh and aged Pd–Rh/Al_2O_3

XPS measurements were performed on aged and freshly-prepared samples and after in situ reduction in pure H_2 at 500 °C. XPS analysis reported in Table 1 reveals on aged Pd–Rh/Al_2O_3 a drop of the atomic Pd/Al ratio ascribed to particle sintering, in line with the drop of metal dispersion measured from H_2 titration measurements. It is worthwhile to notice that particle sintering seems more accentuated on Pd/Al_2O_3 compared to Pd–Rh/Al_2O_3. In the meantime, the atomic Rh/Al ratio is much less affected by the thermal ageing process. In line with the increase of the atomic Rh/Rh + Pd ratio, these trends underline a surface Rh enrichment upon catalyst ageing.

In order to complement XPS analysis which provides an average composition on a depth of 5–10 nm (about a tenth of atomic layers), CO chemisorption was followed by DRIFT to have access

Table 1
Surface characterization and TAP response during NO SP experiments on pre-reduced fresh and aged supported 2.5Pd–0.18Rh/γ-Al_2O_3 catalysts.

Catalyst	Thermal treatment	BET area ($m^2\ g^{-1}_{cata}$)	D[a]	d[b] (nm)	Surf. XPS composition[c]			NO SP experiment[d]	
					Pd/Al	Rh/Al	Rh/Rh + Pd	NO conv.	N_2 Sel.
Pd/Al_2O_3	Fresh	149	0.26	4.3	4.3×10^{-3}			0.10	~0
	Aged	95	0.13	8.8	3.1×10^{-3}			0.38	~0
Pd–Rh/Al_2O_3	Fresh	144	0.31	3.5	6.2×10^{-3}	1.1×10^{-3}	0.15/0.16[e]	0.14	0.54
	Aged	106	0.21	5.4	2.1×10^{-3}	0.7×10^{-3}	0.25	0.31	0.23

[a] Noble metal dispersion estimated from H_2 titration on pre-reduced catalysts assuming H/M = 1.
[b] Average metallic particle size.
[c] Relative accuracy equal to ±20% on the surface atomic M/Al ratio with M = Pd and Rh.
[d] Performed at 350 °C.
[e] From elemental analysis.

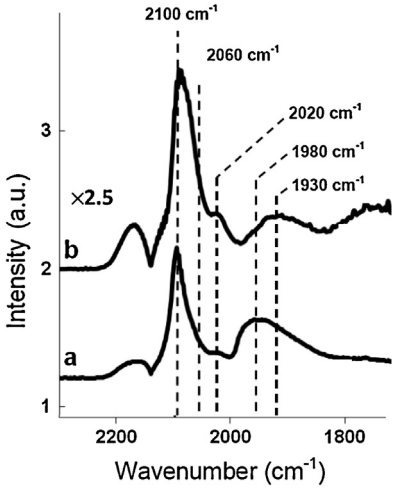

Fig. 1. Infrared spectra of CO adsorbed on pre-reduced Pd–Rh/Al_2O_3 before ageing (a) and after ageing (b).

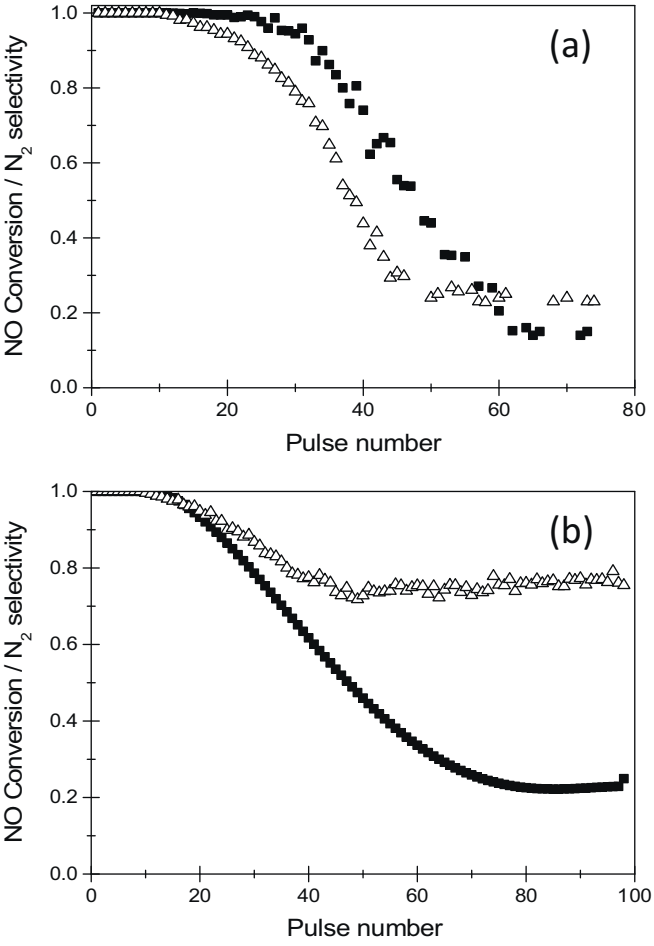

Fig. 2. NO Conversion (■) and selectivity to N_2 production (△) recorded on Pd–Rh/Al_2O_3 at 350 °C (a) and 400 °C (b).

to the effective composition of the outermost layer. Preliminary IR observations on single Pd and Rh catalysts are collected in Fig. S1 (Supplementary materials). They reveal different spectral features with the appearance of a broad contribution located at ~1970 cm^{-1} on Pd/Al_2O_3 coexisting with a narrower one at 2100 cm^{-1} ascribed to multi-coordinated and on-top CO species on metallic Pd sites, respectively [21–24]. On Rh/Al_2O_3, a strong IR band appears at 2060 cm^{-1} currently assigned to CO linearly coordinated to Rh^0. The dissymmetry observed on the signal could be related to a weaker contribution due to the formation of the gem-dicarbonyl structure $Rh^I(CO)_2$ [25–27]. Returning to bimetallic catalysts, the shape of the IR spectrum recorded on the freshly-prepared Pd–Rh/Al_2O_3 is dominated by the characteristic spectral features of Pd/Al_2O_3 (see Fig. 1). A weak contribution is also discernible at 2020 cm^{-1} characteristic of the gem-dicarbonyl structure. Thermal ageing induced a significant attenuation of the overall signal in agreement with a lower dispersion calculated from H_2 chemisorption measurements. A relative increase in intensity for the contribution located at 2100 cm^{-1} with a parallel broadening is discernible whereas the 1980 cm^{-1} IR band shifts to lower wave-number values at ~1930 cm^{-1}. It is also noticeable that the 2020 cm^{-1} IR bands ascribed to the asymmetrical stretching vibration of $Rh^I(CO)_2$ intensifies on the aged sample. Previous workers attempted to identify different contributions on this broad IR band with an apparent maximum at 1930 and 1980 cm^{-1} attributed to CO coordinated to Pd(1 1 1) and Pd(1 0 0) surface planes [21]. In line with this observation, the characteristic IR carbonyl bands for CO on palladium sites attenuates upon ageing, in accordance with the significant surface Rh enrichment previously derived from XPS analysis.

3.2. TAP response during single NO pulse experiments

3.2.1. On freshly-prepared Pd–Rh/Al_2O_3

Prior to single pulse (SP) experiments, the catalyst samples were systematically reduced at 400 °C and subsequently exposed at the selected temperature of 350 or 400 °C to successive NO pulses till the observation of a stable NO conversion regime (Fig. 2). About 40 to 60 pulses are required to reach a pseudo steady state of the catalyst, after a rapid drop of the conversion and selectivity. This behavior can be easily explained by oxygen accumulation from NO dissociation on metallic noble metal sites, which occurs more readily with a rise in temperature. The drop in conversion depends on the quantity of accessible metallic sites and the temperature. At elevated temperature oxygen desorption becomes more significant and creates vacant sites. This correctly explains a higher pseudo steady state conversion at 400 °C and an enhanced N_2 formation reflected by a sharp increase in the N_2 selectivity. The same experiments were performed on monometallic Pd and Rh catalysts at 350 °C revealing a completely different N_2 selectivity behavior for Pd/Al_2O_3 becoming negligible after 30 successive NO pulses (see Fig. 3). From these figures, oxygen balance can be tentatively estimated in order to get some insight in the reaction mechanism. From the inlet NO pulses, the amount of admitted oxygen atoms can be estimated and compared to the amount of O released in the outlet pulses as unconverted NO and N_2O. It was thus found that a large part (corresponding to ~36×10^{17} O atoms) of the inlet oxygen was trapped by Pd–Rh/Al_2O_3 after 60 NO pulses. The density of metallic active sites on freshly prepared Pd–Rh/Al_2O_3 was evaluated as about 10×10^{17} surface atoms. Almost four times more oxygen atoms than surface metal atoms are trapped, suggesting that up to 4 monolayers of the metal particles can be oxidized. Similar trends have been previously reported on Pt/Al_2O_3 [28] and Pt//BaO/Al_2O_3 [29]. Kumar et al. [28] also reported that independent oxygen SP experiments on Pt/Al_2O_3 lead to an oxygen uptake approximately 3–4 times higher than the number of exposed Pt atoms. We repeated these experiments on freshly prepared Pd–Rh/Al_2O_3 at 350 °C by pulsing O_2 instead of NO and found an oxygen uptake of ~7.0×10^{17} O atoms, which corresponds to an oxygen coverage of ~0.7 (assuming O/Me = 1). Thus the oxygen uptake by the catalyst observed during di-oxygen pulses appears to be much lower than during NO SP experiments. Such a statement suggests that besides the O uptake derived from NO dissociation on the metallic

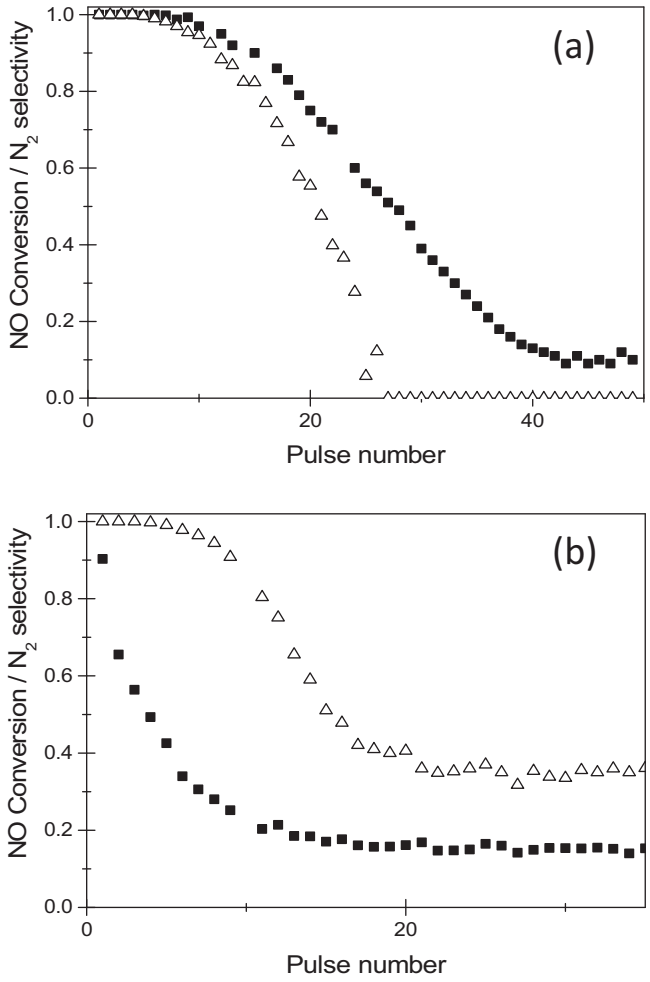

Fig. 3. NO Conversion (■) and selectivity to N_2 production (△) recorded at 350 °C on Pd/Al_2O_3 (a) and on Rh/Al_2O_3 (b).

phase, a significant amount of NO would also be trapped by the alumina support possibly as nitrites or nitrates precursors though no gaseous NO_2 was detected during NO SP experiments. Besides these quantitative aspects derived from the TAP responses integration, some qualitative information can be obtained from the dynamics of these responses, reflecting complex processes associated to surface adsorption, desorption, reactions and the involvement of possible spill-over and reverse spill-over between metals and support phases [20]. By way of illustration, Centi and Arena, previously shown the existence of spillover and reverse spill-over processes on Pt supported over alumina and titania–alumina supports involving nitrito–nitrato species stabilized on the support [30].

Outlet flow rate curves during NO SP experiments carried out on freshly-prepared $Pd–Rh/Al_2O_3$ at 350 °C and 400 °C are reported in Figs. 4a and 5a, respectively. Let us note that for each SP experiment, we observed the NO signal returning to its baseline after 1.5 and 2 s as previously mentioned in the experimental part. Figs. 4 and 5 report the first part of SP experiments up to 0.5 s. It was found that the nitrogen mass balance, calculated from gaseous NO molecules and reaction products from NO dissociation, varies within an acceptable margin of error ±10%. As seen in Fig. 4a, a quite large tailing of the output NO pulse, as compared to the reference Ar pulse, is observable. Since the latter reflects only the gas diffusion within the void volume and the macroporous space of the reactor, such a trend indicates a strong and partly reversible interaction of NO with the catalyst surface. Indeed this reversible NO adsorption is in line with the low extent of NO conversion on $Pd–Rh/Al_2O_3$ at 350 °C (Table 1). This long tailing of the NO response, still occurring when all the N-containing products have been released, can also be related to the possible storage of ad-NO_x species on the alumina phase via a reversible spillover process, as discussed previously [30]. This was also reported elsewhere on lean NO_x trap $Pt/BaO/Al_2O_3$ [31]. Then, one can note an instant and simultaneous production of gaseous N_2O and NO from dissociation and desorption of chemisorbed NO molecules, respectively, while the N_2 response is noticeably delayed afterwards. Similar observations were previously reported by Burch et al. [32] who attributed this delay to successive surface steps involving the conversion of NO to N_2. Indeed, N_2 might be formed by the recombination of adjacent chemisorbed N atoms from NO dissociation. Alternately, this delay between N_2O and N_2 responses can also indicate that N_2 production involves first the formation of N_2O, then its re-adsorption and subsequent dissociation into gaseous nitrogen and surface oxygen, in line with what was proposed by Denton et al. [33]. In that sense, the surface occupancy deriving from competitive adsorptions is likely to control part of the observed selectivity in this complex process. Hence, the likely sequential process for N_2 formation would probably require enough space to occur on the metallic surface, which would be favored by the spillover of adsorbed ad-NO_x intermediates toward the alumina phase, as proposed previously. If one considers now the TAP responses obtained at 400 °C with the freshly-prepared $Pd–Rh/Al_2O_3$ (Fig. 5a), slightly different trends are observed, revealing the extreme sensitivity of the selectivity toward surface reactivity and occupancy. As can be seen, the N_2O release is starting immediately, which is still characteristic of a primary product, but its maximum is much decreased at the benefit of the N_2 release. The major change is that the delay time of N_2 gets shorter as observed in Fig. 5a, but coincides approximately with the initial release of N_2O. This would indicate that by increasing the temperature, the formation of N_2 does not proceed only via a sequential process involving the desorption/readsorption of N_2O, but can proceed also via a direct recombination of N adspecies into N_2. This direct route for N_2 formation might be favored by a faster availability of free adsorption sites from NO desorption, which would increase the relative concentration of chemisorbed N atoms from NO dissociation and then favor their recombination as previously explained [32]. As observed, the long tailing of NO response, previously ascribed to possible storage of ad-NO_x species on the alumina phase, is not modified upon temperature increase.

3.2.2. *On aged $Pd–Rh/Al_2O_3$*

As seen in Fig. 4b, the shape of the outlet flow rate curves differs for all the analyzed products, including the Ar reference curve. A similar effect is observed for all the tested aged samples, as will be seen in Figs. 6 and 7.

Concerning the Ar reference curve, its shift toward longer and broader elution times can be assigned in a first approximation to an increase gas hold-up, due to increased macroporosity of the samples. Since the BET surface area is decreased by about 30% (Table 1) for the aged samples, it can be proposed that for the fresh samples, part of the micro porosity was not accessible to the pulsed gases, while after the sintering obtained by thermal treatment at 980 °C, a new fraction of solid surface is now accessible to the pulsed gases, which creates the observed broadening of the output signals. Alternately, the compact packing of catalyst powder in three-zone reactor could partly explain such broadening of Ar.

The second major change for the aged samples is the marked delay for the release of NO either at 350 or 400 °C. As shown, N_2O signal appears sooner than that of NO on aged samples. This suggests that NO would be more strongly adsorbed and/or NO dissociation previously discussed would occur more readily over noble metals. This explanation seems in relative good agreement with

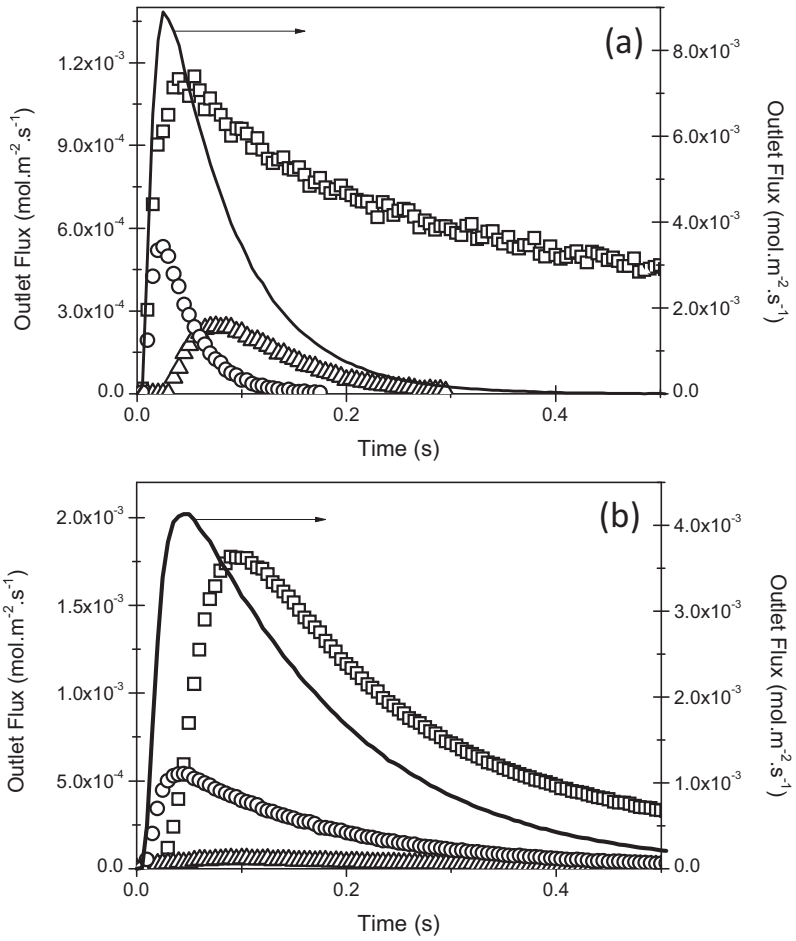

Fig. 4. Outlet flow rate response recorded after NO single pulse TAP experiments at 350 °C on on freshly-prepared Pd–Rh/Al_2O_3 (a) and aged at 980 °C in 10 vol.% H_2O diluted in air (b)—NO (□); N_2O (◯); N_2 (△); solid line represents Ar.

an increase in NO conversion as reported in Table 1. A comparable observation has been earlier reported on Pt/BaO/Al_2O_3 [31] and possibly explained by an interaction of NO with the support or storage component. Parallel to that observation, the delay observed on the production of N_2 on the fresh catalyst becomes shorter at 350 °C even if the N_2 signal strongly attenuates. All those observations emphasize the fact that NO dissociation on metallic sites is much faster than on the freshly-prepared catalyst which seems in correct agreement with the behaviour of a Rh-enriched surface. As a result, further quantification shows that 31% NO is converted vs. 14% on the freshly prepared sample but the selectivity toward N_2 production is lower shifting from 54 to 23% which means that approximately the same amount of nitrogen forms on the fresh and aged samples despite a lower density of active sites. The most prominent observation is related to the opposite trend observed on the spillover process since the long and intense tail observed on the fresh sample still remains but becomes less intense at 350 °C. However, subsequent experiment at 400 °C does not provide a decisive conclusion showing that even if thermal sintering is significant the metal/support would not be significantly altered to completely suppress such spillover process.

In order to get more insight into the impact of the thermal ageing and Rh incorporation on the extent of such spillover process we have repeated the same experiments on monometallic Pd/Al_2O_3 and Rh/Al_2O_3 catalysts at 350 °C (see Figs. S2 and S3 in Supplementary materials) and at 400 °C as illustrated in Figs. 6 and 7. Both samples were submitted to the same thermal ageing process at 980 °C. Compared to Pd–Rh/Al_2O_3, the freshly-prepared Pd/Al_2O_3 exhibits a comparable conversion at 350 °C but is much less selective with the absence of nitrogen formation as indicated in Table 1. Further increase in temperature highlight the same trend in terms of selectivity with only N_2O primarily formed at 400 °C (see Fig. 6a). Thermal ageing affects more significantly the adsorptive properties of Pd/Al_2O_3 than Pd–Rh/Al_2O_3. But the most prominent information is likely related to a significant attenuation of the long tail observed on the NO outlet flow rate profile compared to Pd–Rh/Al_2O_3 at 350 °C and also 400 °C.

CO adsorption measurements lead to IR spectra having an extremely low intensity on aged Pd/Al_2O_3 and more markedly on aged Rh/Al_2O_3 (not shown) which corroborates a more extensive loss of metal dispersion than on aged Pd–Rh/Al_2O_3. Intriguingly, the conversion recorded on aged Pd/Al_2O_3 during NO SP experiment becomes higher than on the fresh sample at 350 °C, but is not accompanied with significant enhancement in N_2 production via the readsorption of N_2O as evidenced in Fig. S2. Such tendency is confirmed at 400 °C. Hence, the second specific feature which differentiates single Pd and bimetallic Pd–Rh catalysts is the selectivity toward nitrogen which emphasizes the role of rhodium in the formation of significant extent of N_2 on Pd–Rh/Al_2O_3 even after ageing. NO SP experiments on Rh/Al_2O_3 are consistent with the above-mentioned comments for which N_2 predominantly formed on the fresh sample while it is still primary formed on aged sample but in lower extent (Fig. 7). Finally, it is also remarkable that the slow NO desorption process completely disappears which might have different origins in the case of rhodium based catalyst related to particle sintering but also to partial diffusion of oxidic Rh species

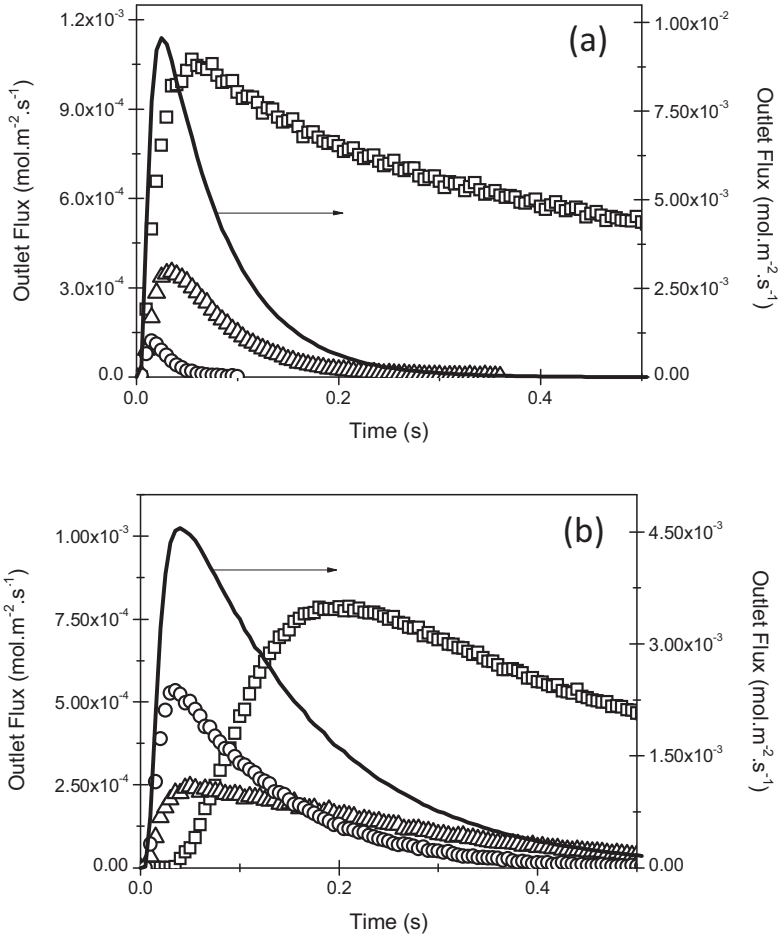

Fig. 5. Outlet flow rate response recorded after NO single pulse TAP experiments at 400 °C on freshly-prepared Pd–Rh/Al_2O_3 (a) and aged at 980 °C in 10 vol.% H_2O diluted in air (b)—NO (□); N_2O (◯); N_2 (△); solid line represents Ar.

in the alumina support leading to the formation of diffuse bulk aluminate species.

3.3. General assessments

This study investigated the impact of thermal ageing on the adsorptive properties of NGV bimetallic Pd–Rh/Al_2O_3 catalysts toward NO combining FTIR CO adsorption and XPS analysis. It was found that NO single pulse TAP measurements provide information that reflects chemical processes taking place at the metal/support interface and onto metallic noble metal particles. Both are sensitive to ageing at 980 °C in wet atmosphere due to the occurrence of particle sintering, modifications of the morphology of the particles and changes in surface composition with the consequence to alter the outlet flow rate profiles of NO and reaction products N_2 and N_2O. All these phenomena may have some consequences on the extent of NO dissociation recognized as structure sensitive [13].

Returning to the examination of NO SP experiments in all cases, we observe for short time responses fast chemical processes associated to NO desorption and a parallel production of N_2 and N_2O over noble metals afterwards a slow NO desorption process is usually observed which does not coincide to N_2 and N_2O production. As previously observed, Pd–Rh/Al_2O_3 is able to store oxygen and ad-NO_x species in larger amount than that requested for the saturation of the metallic Pd and Rh sites. This latter observation suggests the involvement of slow spillover from the metal to the alumina support and reverse spillover processes with subsequent gaseous NO formation through desorption/decomposition. Such an explanation is related to the extent of the metal/support interface i.e. the noble metal dispersion [31]. Indeed, Kabin et al. found on lean-NO_x trap Pt/BaO/Al_2O_3 that the Pt–Ba interface is critical for NO_x storage and demonstrated that the specific interfacial perimeter p_{Pt}/a_{Pt}, between Pt and Ba is a quantitative measure of the of the Pt–Ba interface observing a minimum in normalized NO_x uptake for the lowest specific interfacial perimeter. p_{Pt}/a_{Pt} can be calculated according to Eq. (1) which accounts for the specific noble metal surface a_{Pt} (nm^2/g) and the perimeter p_{Pt} (nm/g) given by Eqs. (2) and (3) where n_{Pt} and d_{Pt} denote for the number of noble metal per g of catalyst and the average particle size, respectively [31].

$$\frac{p_{Pt}}{a_{Pt}} = \frac{4}{d_{Pt}} \quad (1)$$

$$a_{Pt} = n_{Pt}\frac{\pi d_{Pt}^2}{4} \quad (2)$$

$$p_{Pt} = n_{Pt}\pi d_{Pt} \quad (3)$$

Returning to our observations, one can observe from Fig. 8 that the amount of NO desorbed from the catalyst varies linearly with the specific interfacial perimeter according to the margin of error with a weak dependence on the temperature. Such relationship seems also consistent with previous investigations of methane adsorption on the same catalysts with spillover process weakly activated taking place during methane chemisorption. The same observations on the profile of the outlet flow rate of H_2 have been

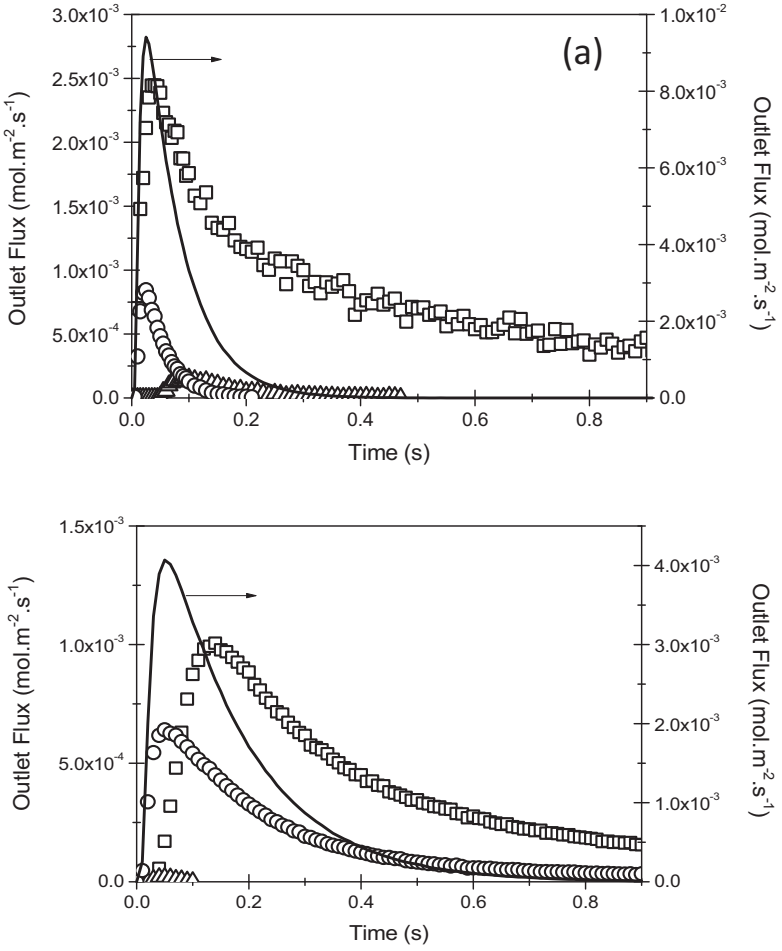

Fig. 6. Outlet flow rate response recorded after NO single pulse TAP experiments at 400 °C on freshly-prepared Pd/Al_2O_3 (a) and aged at 980 °C in 10 vol.% H_2O diluted in air (b)—NO (□); N_2O (○); N_2 (△); solid line represents Ar.

reported with fast methane dissociation and the appearance of a long tail ascribed to a slow H_2 production through the participation of OH groups via a spillover from the alumina support recognized as a reservoir of OH groups onto metallic noble metal sites [9].

As above-mentioned, the first part of NO SP experiments, corresponding to a fast desorption of NO and reduction products, would be more related to chemical processes taking place over metallic Pd and Rh sites. Preliminary observations on single Pd and Rh catalysts point out drastic changes in selectivity behavior with the absence of N_2 formation on Pd compared to Rh. For $Pd–Rh/Al_2O_3$, two borderlines cases can be envisioned concerning the adsorptive properties of the resulting bimetallic catalysts often depending on the preparation method utilized with preferential segregation of Pd and Rh on alumina and/or the formation of alloyed and/or bimetallic Pd–Rh particles. Hence, depending on the preparation method the results can be discussed in terms of geometric or electronic effects. In the former case, weak interaction of Pd and Rh can lead to the preservation of their peculiar adsorptive properties while they can be drastically changed in the case of alloyed particles when they strongly interact. To continue the discussion let us remind that Pd and Rh loading differ with larger amount of Pd (2.5 wt.% vs. 0.18 wt.% of Rh). As a consequence, CO chemisorption measurements reveal similar spectral features on Pd/Al_2O_3 and $Pd–Rh/Al_2O_3$ characteristic of Pd. Such similarity is still observable in NO conversion but strong divergences appear by examining the selectivity behavior in favor of nitrogen production at 400 °C on $Pd–Rh/Al_2O_3$ while Pd/Al_2O_3 is unable to produce N_2 contrarily to Rh. This means that NO dissociation, and recombination between NO and N adsorbed species or between two adjacent chemisorbed N atoms governing the selectivity behavior on $Pd–Rh/Al_2O_3$ would occur more preferentially on Rh. As a matter of fact, such a result seems in relative good agreement with steady-state rate measurements performed during the NO/H_2 on the same catalysts which show that predicted rates can be modeled taking into account non-competitive adsorptions with preferential adsorption of NO on Rh and H_2 on Pd and a nearest vacant site for NO dissociation mostly composed of Pd [3]. Hence, dissociated N atoms and NO molecules on Rh would be the sole ad-species responsible of the formation of N_2 and N_2O.

Thermal ageing induces significant changes with a surface Rh enrichment evidenced from XPS analysis and confirmed from FTIR CO adsorption measurements. IR spectrum on the aged $Pd–Rh/Al_2O_3$ shows that parallel to a decrease in the density of metallic sites, a relative increase in the 2020 cm^{-1} IR band ascribed to gem-dicarbonyl species is observable. An important observation is also related to the fact that the overall signal is much more intense than that obtained on Pd/Al_2O_3 and Rh/Al_2O_3 for which no signal was detected suggesting that Rh incorporation to Pd slower particle sintering. This can correctly explain why the spillover process is less attenuated on aged $Pd–Rh/Al_2O_3$ than on aged Pd/Al_2O_3 and Rh/Al_2O_3. As a consequence, an appreciable Rh enrichment would characterize aged-$Pd–Rh/Al_2O_3$ which can explain a stronger NO adsorption as previously discussed. This latter information is of significant importance and can correctly explain the changes observed on the selectivity behavior on freshly-prepared and aged $Pd–Rh/Al_2O_3$ during the short period

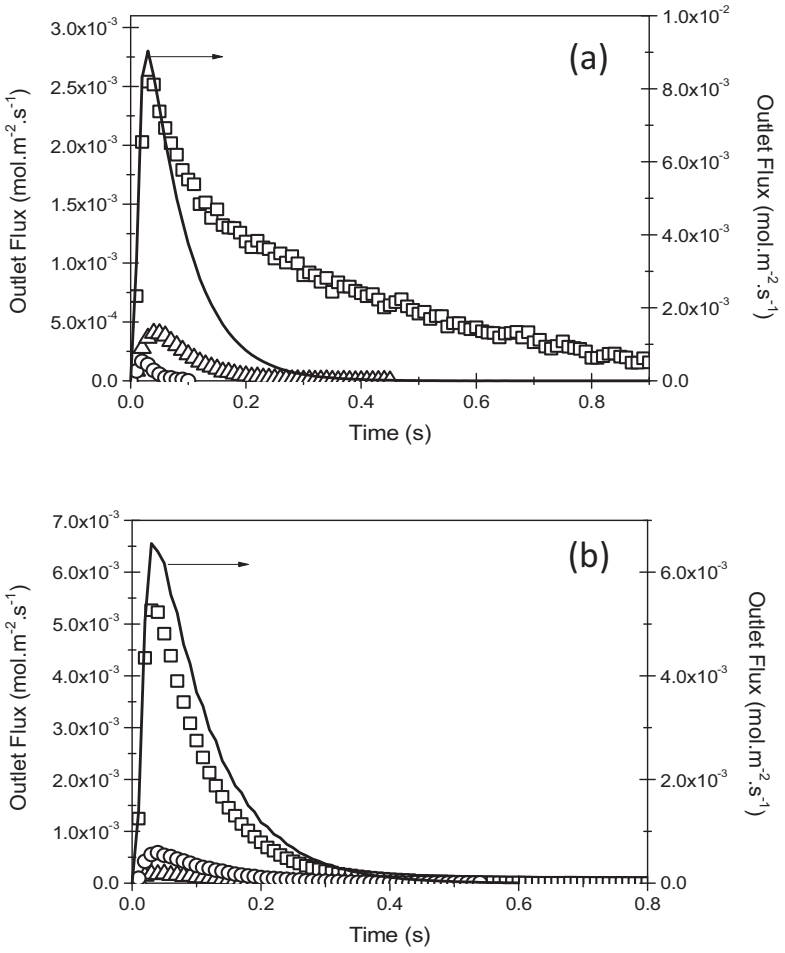

Fig. 7. Outlet flow rate response recorded after NO single pulse TAP experiments at 400 °C on freshly-prepared Rh/Al_2O_3 (a) and aged at 980 °C in 10 vol.% H_2O diluted in air (b)—NO (□); N_2O (○); N_2 (△); solid line represents Ar.

corresponding to the fast NO desorption. As illustrated in Fig. 9, N_2 selectivity increases when NO desorption evolves on $Pd–Rh/Al_2O_3$. This can be related to a more extensive NO dissociation when vacant nearest neighbor sites are released leading to high N coverage. Consequently, the recombination of chemisorbed N atoms would preferably explain N_2 formation on freshly-prepared $Pd–Rh/Al_2O_3$. On the other hand, similarly to Rh/Al_2O_3, N_2 selectivity is quite independent of NO pressure during this short period on the aged-bimetallic catalyst. The weak NO partial pressure dependency has been the subject of numerous investigations [34–36] in the past essentially from steady-state experiments at atmospheric pressure taking into account the following step as possible pathways for N_2 and N_2O formation where $*$ stands for a vacant site.

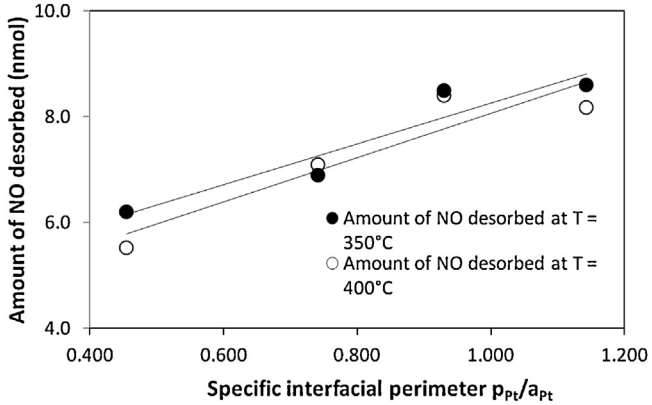

Fig. 8. Plot of the amount of NO desorbed during SP experiments vs. the specific interfacial perimeter.

$$NO + * \rightarrow N_{ads} + O_{ads} \quad (4)$$

$$NO + N_{ads} \rightarrow N_2O + * \quad (5)$$

$$NO + N_{ads} \rightarrow N_2 + * + O_{ads} \quad (6)$$

$$N_{ads} + N_{ads} \rightarrow N_2 + 2* \quad (7)$$

Basically, N_2 Selectivity depends on the relative rate r_{N_2}/r_{N_2O}. Hence, Eq. (8) can be easily derived taking into account the steps for the formation of N_2 and N_2O and then Eq. (9) can be demonstrated from the steady-state approximation to chemisorbed N atoms as described elsewhere [35–37].

$$\frac{r_{N_2}}{r_{N_2O}} = \frac{k_7}{k_5}\frac{\theta_N}{\theta_{NO}} + \frac{k_6}{k_5} \quad (8)$$

$$\frac{4r_{N_2}}{r_{N_2O}} = \frac{(k_6+k_5)}{k_5}\left(\sqrt{1+\frac{8k_7k_4}{(k_6+k_5)^2K_{NO}P_{NO}}} + \frac{3k_6}{k_5} - 1\right) \quad (9)$$

By examining Eq. (9) r_{N_2}/r_{N_2O} becomes independent on NO pressure if the term $8k_7k_4/(k_6+k_5)^2K_{NO}P_{NO}$ becomes almost nil which means a high numeric value for K_{NO} and rate constants k_5 and k_6 much higher than k_7 and k_4. Hence, N_2 selectivity is governed by the strength of NO adsorption and the reactivity of nitrosyl species. This

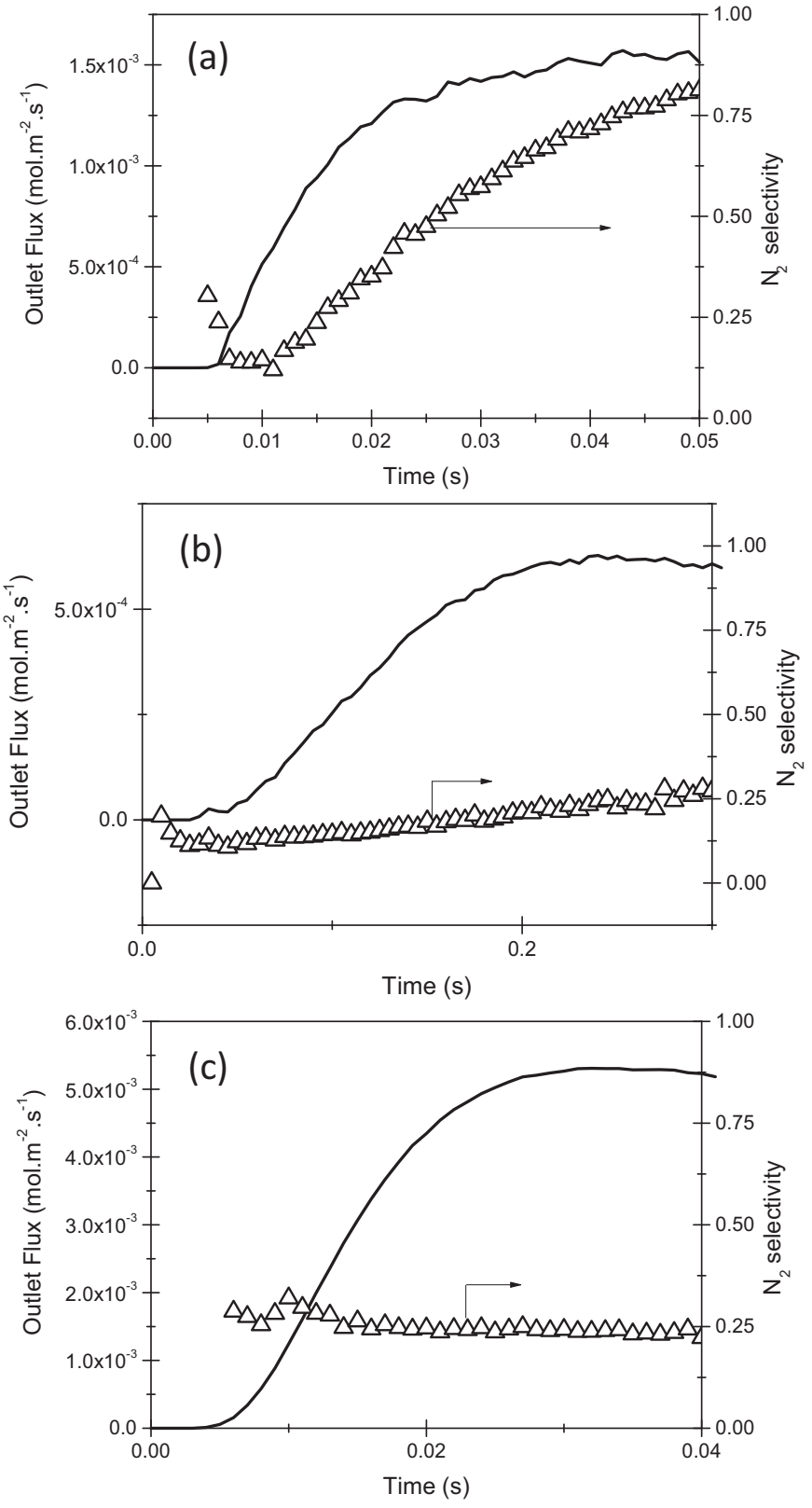

Fig. 9. Plot of N_2 selectivity and NO flow rate vs. time at the beginning of NO SP experiments on freshly-prepared Pd–Rh/Al_2O_3 (a); aged Pd–Rh/Al_2O_3 (b); aged Rh/Al_2O_3: ··· NO flow rate, (△) N_2 selectivity.

is consistent with previous statements on the fresh bimetallic sample. Now, regarding the N_2 selectivity of the aged Pd–Rh/Al_2O_3 and Rh/Al_2O_3 from NO SP TAP experiments (see Fig. 9), one can observe similar behaviors with N_2 selectivity remaining weakly sensitive to change in NO partial pressure. This observation emphasizes the fact that at high NO coverage due stronger NO adsorption on Rh and less reactive nitrosyl species toward NO dissociation on aged samples, the production of nitrogen will occur preferably via step (5)

similarly to Rh/Al_2O_3. Hence, r_{N_2}/r_{N_2O} on aged $Pd–Rh/Al_2O_3$ will also depend on the rate constant relative to steps (5) and (6).

4. Conclusion

This study reports a TAP investigation of NO adsorption on bimetallic $Pd–Rh/Al_2O_3$. Particular attention was paid to the influence of thermal ageing on the adsorptive properties of noble metals. The profile of the outlet flow rate of NO characterizes the involvement of fast processes such as NO adsorption/dissociation and surface reactions taking place over noble metals and leading to the predominant release of N_2O on freshly-prepared catalysts and a significant delay in N_2 production. In parallel, a slow step has been characterized and ascribed to the occurrence of spillover process of ad-NO_x species on the alumina support depending on the specific interfacial parameter of noble metal particles.

It was found that thermal ageing at 980 °C strongly affects the fast and slow NO desorption underlining the key role of Rh in both processes. The conjunction of morphological changes affecting NO dissociation of Pd and surface Rh enrichment leads to a Rh like behavior for the aged $Pd–Rh/Al_2O_3$. Indeed, an increase in NO conversion associated to a poorer N_2 formation would be likely due to the stabilization of more strongly chemisorbed NO species possibly on $Rh^{\delta+}$. In parallel, particle sintering alters the specific interfacial perimeter weakening spillover process especially on Pd/Al_2O_3. Interesting, Rh incorporation to Pd would preserve the metal/support interaction on aged $Pd–Rh/Al_2O_3$.

Acknowledgemnts

We would like to thank the Ademe for a grant (Y. Renème) and Umicore company for supplying the catalyst. The laboratory participates in the Institut de Recherche en Environnement Industriel (IRENI) which is financed by the Communauté Urbaine de Dunkerque, the Région Nord Pas-de-Calais, the Ministère de l'Enseignement Supérieur et de la Recherche, the CNRS and European Regional Development Fund (ERDF).

Appendix A. Supplementary data

Supplementary material related to this article can be found, in the online version, at http://dx.doi.org/10.1016/j.apcatb.2014.05.046.

References

[1] M. Salaün, A. Kouakou, S. Da Costa, P. Da Costa, Appl. Catal., B: Environ. 88 (2009) 386–397.
[2] F. Klingstedt, A.K. Neyestanaki, R. Byggningsbacka, L.-E. Lindfors, M. Lundén, M. Petersson, P. Tengström, T. Ollonqvist, J. Väyrynen, Appl. Catal., A: Gen. 209 (2001) 301–316.
[3] Y. Renème, F. Dhainaut, P. Granger, Appl. Catal., B: Environ. 111–112 (2012) 424–432.
[4] P. Gélin, L. Urfels, M. Primet, E. Tena, Catal. Today 83 (2003) 45–57.
[5] D. Bounechada, G. Groppi, P. Forzatti, K. Kallinen, T. Kinnunen, Appl. Catal., B: Environ. 119–120 (2012) 91–99.
[6] G. Karavalakis, T.D. Durbin, M. Villela, J. Wayne Miller, J. Nat. Gas Sci. Eng. 4 (2012) 8–16.
[7] J.P. Breen, C. Rioche, R. Burch, C. Hardacre, F.C. Meunier, Appl. Catal., B: Environ. 72 (2007) 178–186.
[8] Y. Renème, F. Dhainaut, P. Granger, Top. Catal. 52 (2009) 2007–2012.
[9] Y. Renème, F. Dhainaut, S. Pietrzyk, M. Chaar, A.C. van Veen, P. Granger, Appl. Catal., B: Environ. 126 (2012) 239–248.
[10] M.M. Wolf, H. Zhu, W.H. Green, G.S. Jackson, Appl. Catal., A: Gen. 244 (2003) 323–340.
[11] E. Becker, P.A. Carlsson, H. Grönbeck, M. Skoglundh, J. Catal. 252 (2007) 11–17.
[12] P. Granger, L. Delannoy, L. Leclercq, G. Leclercq, J. Catal. 177 (1998) 147–151.
[13] C.H.F. Peden, D.N. Belton, S.J.J. Schmieg, J. Catal. 155 (1995) 204–218.
[14] J.T. Gleaves, J.B. Ebner, T.C. Kuechler, Catal. Rev. Sci. Eng. 30 (1988) 49–116.
[15] A. Sukev, A.C. van Veen, A. Toktarev, E. Sadovskaya, B. Bal'zhinimaev, C. Mirodatos, Catal. Commun. 5 (2004) 691–695.
[16] Y. Renème, F. Dhainaut, M. Frère, L. Gengembre, P. Granger, C. Dujardin, P. De Cola, Surf. Interface Anal. 42 (2010) 530–535.
[17] C.M. Mendez, H. Olivero, D.E. Damiani, M.A. Volpe, Appl. Catal., B: Environ. 84 (2008) 156–161.
[18] D.A. Shirley, Phys. Rev. B: Condens. Matter 5 (12) (1972) 4709–4714.
[19] A.S. Mamede, G. Leclercq, E. Payen, P. Granger, L. Gengembre, J. Grimblot, Surf. Interface Anal. 34 (2002) 105–111.
[20] J.T. Gleaves, G.S. Yablonskii, P. Phanawadee, Y. Schuurman, Appl. Catal., A: Gen. 160 (1997) 55–88.
[21] C. Binet, A. Jadi, J.C. Lavalley, J. Chim. Phys. Biol. 86 (1989) 451–470.
[22] D. Roth, P. Gélin, A. Kaddouri, E. Garbowski, M. Primet, E. Tena, Catal. Today 112 (2006) 134–138.
[23] P. Granger, H. Praliaud, J. Billy, L. Leclercq, G. Leclercq, Surf. Interface Anal. 34 (2002) 92–96.
[24] C. Neyertz, M. Volpe, D. Perez, I. Costilla, M. Sanchez, C. Gigola, Appl. Catal., A: Gen. 368 (2009) 146–157.
[25] R.R. Cavanagh, J.T. Yates, J. Chem. Phys. 74 (1981) 4150–4155.
[26] D.A. Buchanan, M.E. Fernandez, F. Solymosi, J.M. White, J. Catal. 125 (1990) 456–466.
[27] J.A. Anderson, C.H. Rochester, J. Chem. Soc., Faraday Trans. 87 (9) (1991) 1479–1483.
[28] A. Kumar, V. Medhekar, M.P. Harold, V. Balakotaiah, Appl. Catal., B: Environ. 90 (2009) 642–651.
[29] V. Medhekar, V. Balakotaiah, M.P. Harold, Catal. Today 121 (2007) 226–236.
[30] G. Centi, G.E. Arena, J. Mol. Catal. A: Chem. 204–205 (2003) 663–671.
[31] K.S. Kabin, P. Khanna, R.L. Muncrief, V. Medhekar, M.P. Harold, Catal. Today 114 (2006) 72–85.
[32] R. Burch, P.J. Millington, A.P. Walker, Appl. Catal., B: Environ. 4 (1994) 65–94.
[33] P. Denton, Y. Schuurman, A. Giroir-Fendler, H. Praliaud, M. Primet, C. Mirodatos, Stud. Surf. Sci. Catal. 130 (2000) 1277–1282.
[34] B.K. Cho, J. Catal. 138 (1992) 255–266.
[35] P. Granger, P. Malfoy, L. Leclercq, G. Leclercq, J. Catal. 223 (2004) 142–151.
[36] F. Dhainaut, S. Pietrzik, P. Granger, J. Catal. 258 (2008) 296–305.
[37] D.N. Belton, S.J. Schmieg, J. Catal. 144 (1993) 9–15.